Structural, Morphological, and Oxygen Handling Properties of Nanosized Cerium−Terbium Mixed Oxides Prepared by Microemulsion

A. B. Hungría,[†] A. Martínez-Arias,*[,†] M. Fernández-García,[†] A. Iglesias-Juez,[†] A. Guerrero-Ruiz,[‡] J. J. Calvino,[§] J. C. Conesa,[†] and J. Soria[†]

Instituto de Catálisis y Petroleoquímica, CSIC, Campus Cantoblanco, C/Marie Curie, 28049 Madrid, Spain, Departamento de Química Inórganica y Técnica, UNED, 28040 Madrid, Spain, and Departamento de Ciencia de los Materiales e Ingeniería Metalúrgica y Química Inorgánica, Facultad de Ciencias, Universidad de Cádiz, 11510 Puerto Real, Cádiz, Spain

Received January 29, 2003. Revised Manuscript Received June 11, 2003

The structural/morphological and oxygen handling properties of two high-surface-area Ce−Tb mixed oxides prepared by a microemulsion method with Ce/Tb atomic ratios of ca. 4 and 1 have been analyzed in a multitechnique study (HREM, XEDS, XRD, Raman, XPS, O_2^--EPR, adsorbed methoxy IR, and $C^{18}O_2$ isotopic exchange). Agglomerates of mixed-oxide nanoparticles (average size in the 5−7 nm range) with cubic fluorite structure are shown to be formed with varying lattice parameters as a function of the amount of Tb^{3+} and associated intrinsic oxygen vacancy defects present in each case. A trend toward stabilization of higher relative amounts of Tb^{4+} with increasing the Tb content of the mixed oxide is inferred from analysis of XRD and Raman results. Oxygen is shown to chemisorb as superoxide species on the outgassed samples. EPR analysis of these species shows that terbium promotes generation of clustered vacancies defects at the surface of the mixed-oxide nanoparticles, in agreement with adsorbed methoxy IR experiments. Employment of $C^{18}O_2$ as a tracer molecule in isotopic exchange experiments suggests that oxygen bulk diffusion is moderately altered upon Tb doping of ceria, slightly decreasing with increasing the Tb content of the mixed-oxide nanoparticles.

I. Introduction

The properties of mixed oxide solid compounds depend on a series of factors, among which the particle size, the structural characteristics, and the chemical nonstoichiometry are of capital importance.[1,2] The case of ceria-based mixed oxides has technological implications for the present and future improvements of three-way catalysts,[3,4] as well as of oxygen permeation membranes, oxygen gas sensors, and fuel cells electrolytes and electrodes.[4−7] In particular, ceria modification by doping with terbium has shown to lead to materials with enhanced catalytic properties for oxidation reactions as well as improved redox properties in terms of presenting both a higher oxygen storage capacity and a higher ability to attenuate oscillations of the oxygen partial pressure in the reacting environment,[8−10] both properties of major interest in the three-way catalysts field.[3,4] Additionally, Ce−Tb mixed-oxide materials present electrical properties of mixed conductors (ionic and electronic) at relatively low temperature, which depend on the chemical composition of the solid.[11] This can be of interest for their potential use as electrode components for intermediate- or low-temperature fuel cells as well as for oxygen membranes.[6,11] On the other hand, nanoparticle configurations of these materials are interesting from a catalytic point of view as they naturally possess a higher surface-to-volume ratio and could present improved redox properties, related to a higher facility for oxygen vacancies generation.[4,12,13] Besides, employment of preparation methods leading to homodisperse nanoparticles can allow, in contrast to solid-state synthesis techniques, decrease of the sintering temperatures required to obtain dense materials with optimum conducting properties for electrolytic mem-

* Corresponding author. E-mail: amartinez@icp.csic.es. Fax: 34 91 5854760.

[†] Instituto de Catálisis y Petroleoquímica, CSIC, Campus Cantoblanco, C/ Marie Curie.

[‡] Departamento de Química Inórganica y Técnica, UNED.

[§] Universidad de Cádiz.

(1) Che, M.; Bennet, C. O. *Adv. Catal.* **1989**, *36*, 55.

(2) Kofsta, P. *Non-stoichiometry, Diffusion and Electrical Conductivity of Binary Mixed Oxides*; Wiley: New York, 1972.

(3) Kašpar, J.; Fornasiero, P.; Graziani, M. *Catal. Today* **1999**, *50*, 285.

(4) Trovarelli, A., Ed. *Catalysis by Ceria and Related Materials*; Imperial College Press: London, 2002.

(5) Stoukides, M. *Catal. Rev. Sci. Eng.* **2000**, *42*, 1.

(6) Steele, B. C. H. *Solid State Ionics* **2000**, *134*, 3.

(7) Tschöpe, A.; Schaadt, D.; Birringer, R.; Jing, J. Y. *Nanostruct. Mater.* **1997**, *9*, 423.

(8) Zamar, F.; Trovarelli, A.; de Leitenburg, C.; Dolcetti, G. *Stud. Surf. Sci. Catal.* **1996**, *101*, 1283.

(9) Bernal, S.; Blanco, G.; Cauqui, M. A.; Corchado, P.; Pintado, J. M.; Rodríguez-Izquierdo, J. M. *Chem. Commun.* **1997**, 1545.

(10) Bernal, S.; Blanco, G.; Cauqui, M. A.; Corchado, M. P.; Larese, C.; Pintado, J. M.; Rodríguez-Izquierdo, J. M. *Catal. Today* **1999**, *53*, 607.

(11) Shuk, P.; Greenblatt, M.; Croft, M. *Chem. Mater.* **1999**, *11*, 473.

(12) Tsunekawa, S.; Ishikawa, K.; Li, Z.-Q.; Kawazoe, Y.; Kasuya, Y. *Phys. Rev. Lett.* **2000**, *85*, 3440.

(13) Spanier, J. E.; Robinson, R. D.; Zhang, F.; Chan, S.-W.; Herman, I. P. *Phys. Rev. B* **2001**, *64*, 245407-1.

10.1021/cm031028n CCC: $25.00 © 2003 American Chemical Society
Published on Web 10/02/2003

branes.[11,14] In this respect, the spatial confinement within aqueous droplets in reverse microemulsions, which act as synthesis microreactors, can provide the ideal conditions for the development of most optimum structural/morphological properties during preparation of these nanosized materials.[15,16]

In the present work, two nanosized Ce−Tb mixed oxides with Ce/Tb atomic ratios of 4 and 1 have been synthesized. The preparation method is based on coprecipitation of the Ce and Tb cations within reverse microemulsions. In previous work, it has been shown that employment of this preparation method can allow a precise control of the particle size for materials of this kind, yielding narrow nanosized distributions, as well as a rigorous control (at least much better, in principle, than employing conventional coprecipitation methods)[17] of the chemical composition at a molecular scale.[18,19] The study intends to give a picture on the structural, morphological, and oxygen handling properties of the materials prepared by the mentioned microemulsion method in order to get information on the potentialities of these materials for their use in the mentioned applications.

II. Experimental Section

Two samples were prepared by a microemulsion method with initial Ce/Tb atomic ratios of 4 and 1 in the reacting mixtures. The corresponding Ce(III) and Tb(III) nitrates (Aldrich) were introduced in a reverse microemulsion (water in oil) using *n*-heptane as the organic phase, Triton X-100 (Aldrich) as surfactant, and hexanol as cosurfactant. This suspension was mixed with another one (having similar characteristics in terms of the essential components concentrations) containing as aqueous phase an alkali solution (TMAH, Aldrich). The resulting mixtures, with all cations coprecipitated, were stirred for 24 h, centrifuged, decanted, and rinsed with methanol. After drying the resulting solid overnight at 353 K, it was calcined under air at 773 K for 2 h. The overall conditions employed during these preparations were similar to those reported in a previous work,[19] to which the reader is referred for further details. The corresponding materials will be hereafter referred to as CeTb4 and CeTb1 (in correlation with the corresponding atomic ratios). Chemical analysis (by ICP-AES) showed Ce/Tb atomic ratios of 3.93 and 1.10 for CeTb4 and CeTb1, respectively; this indicated that (within experimental error) quantitative precipitation of both cerium and terbium cations was achieved. Cerium oxide (CeO_2) and terbium oxide (TbO_x) references were prepared following the same procedure. Specific surface areas obtained by the BET method were 92, 104, 95, and 14 $m^2\ g^{-1}$ for CeO_2, CeTb4, CeTb1, and TbO_x, respectively.

Powder X-ray diffraction (XRD) patterns were recorded on a Siemens D-500 diffractometer using nickel-filtered Cu Kα radiation and operating at 40 kV and 25 mA. Spectra were taken with a 0.025° step size and using a counting time of 1 s per point. Fitting of the full diffractograms was carried out with the PowderCell program and took into account both Cu $K\alpha_1$ and $K\alpha_2$ lines of the radiation used.[20]

High-resolution electron microscopy (HREM) images were recorded in a JEOL 2000 EX microscope, equipped with a top entry specimen holder, with 0.21-nm point to point resolution. The experimental micrographs were digitized using a CCD camera COHU-4910. Digital image processing was performed by using the SEMPER 6+ software. X-ray energy-dispersive spectroscopy (XEDS) experiments were carried out using a JEOL 2000 FX system equipped with a LINK (AN 10000) probe for energy-dispersive X-ray spectroscopy analysis. Sample spot for XEDS analysis is about 100 nm. For HREM and XEDS experiments, portions of sample were crushed in an agate mortar and suspended in hexanol. After ultrasonic dispersion, a droplet was deposited on a copper grid supporting a perforated carbon film.

Raman spectra were obtained at room temperature (RT) with a Bruker RFS-100 FT-Raman spectrometer provided with a diode-pumped germanium solid-state detector which operates at liquid nitrogen temperature. A Nd:YAG laser (1064 nm) was used as excitation source at a power of 100 mW. Powdered samples were pressed in a holder and analyzed (500 scans, 4 cm^{-1} resolution) without further treatment.

Photoelectron spectra were acquired with a VG ESCALAB 200R spectrometer equipped with a hemispherical electron analyzer and an Al Kα 120 W X-ray source. The powder samples were pressed into small aluminum cylinders and then mounted on a sample rod placed in an in-situ pretreatment chamber and treated thoroughly under vacuum at RT and for 1 h at 473 K followed by treatment under O_2 at 473 K prior to being moved into the analysis chamber adjacent to the pretreatment one. The pressure in the ion-pumped analysis chamber was maintained below 3×10^{-9} Torr (1 Torr = 133.33 N m^{-2}) during data acquisition. The intensities were estimated by calculating the integral of each peak (or a set of them) after subtraction of the "S-shaped" Shirley-type background and using experimental sensitivity factors from the literature.[21] Considering the severe overlapping of the C(1s) peaks (which are small, due to the relatively low hydrocarbon chemisorption capacity of these oxides of low acidity and the sample pretreatment) with the Ce(4s) and Tb($4p_{3/2}$) lines, energies were referenced to the Ce(3d) u‴ peak, taken to appear at 916.7 eV,[22] and which, as verified by principal component analysis, normally does not change on reduction or mixed oxide formation.[23]

FTIR experiments were performed at RT with a Nicolet 5ZDX Fourier transform spectrometer, with a resolution of 4 cm^{-1} and accumulating 256 scans. For methanol adsorption experiments, thin self-supporting disks (ca. 10 mg cm^{-2}) were prepared by pressing the powders at 1 t cm^{-2} and handled in standard greaseless cells. Before methanol chemisorption, the sample was calcined at 773 K for 1 h in pure oxygen followed by outgassing at 773 K for 1 h. Then, methanol was adsorbed at RT followed by outgassing at 373 K. The samples were also examined in pellets diluted with KBr, using a weight ratio of catalyst/KBr = 1:199.

Electron paramagnetic resonance (EPR) spectra were recorded at 77 K with a Bruker ER 200 D spectrometer operating in the X-band and calibrated with a DPPH standard (g = 2.0036). Portions of ca. 40 mg were placed inside a quartz probe cell with greaseless stopcocks. A conventional dynamic high-vacuum line was used for vacuum or adsorption treatments. The samples were in all cases precalcined under 300 Torr of O_2 at 773 K for 2 h. Following this treatment, the samples were outgassed at 773 K prior to oxygen adsorption. Oxygen adsorption was performed by admission of a dose of 70 μmol

(14) Kleinlogel, C.; Gauckler, L. J. *Solid State Ionics* **2000**, *135*, 567.
(15) Schwuger, M.-J.; Stickdorn, K.; Schomäcker, R. *Chem. Rev.* **1995**, *95*, 849.
(16) Zarur, A. J.; Ying, J. Y. *Nature* **2000**, *403*, 65.
(17) Rossignol, S.; Madier, Y.; Duprez, D. *Catal. Today* **1999**, *50*, 261.
(18) Iglesias-Juez, A.; Hungría, A. B.; Gálvez, O.; Martínez-Arias, A.; Fernández-García, M.; Guerrero-Ruiz, A.; Conesa, J. C.; Soria, J. *Stud. Surf. Sci. Catal.* **2001**, *138*, 347.
(19) Martínez-Arias, A.; Fernández-García, M.; Ballesteros, V.; Salamanca, L. N.; Otero, C.; Conesa, J. C.; Soria, J. *Langmuir* **1999**, *15*, 4796.
(20) Kraus, W.; Nolze, G. *Powder Cell for Windows* v. 2.3; program described and available at Internet URL http://www.bam.de/service/download/download.htm.
(21) Wagner, C. D.; Davis, L. E.; Teller, M. V.; Taylor, J. A.; Raymond, R. M.; Gale, L. H.; *Surf. Interface Anal.* **1981**, *3*, 211.
(22) Laachir, A.; Perrichon, V.; Badri, A.; Lamotte, J.; Catherine, E.; Lavalley, J. C..; El Fallah, J.; Hilaire, L.; le Normand, F.; Quéméré, E.; Sauvion, G. N.; Touret, O. *J. Chem. Soc., Faraday Trans.* **1991**, *87*, 1601.
(23) Martínez-Arias, A.; Fernández-García, M.; Hungría, A. B.; Conesa, J. C.; Munuera, G. *J. Phys. Chem. B* **2003**, *107*, 2667.

Table 1. HREM/XEDS/XRD Main Results (See Text for Details)

sample	cell parameter (Å)[a]	particle size (nm) HREM[b]	particle size (nm) XRD[a]	$(Ce/Tb)_{at.}$[c]
CeO_2	5.4092	6.7 (8.2)	7.9	
CeTb4	5.4006	6.6 (9.0)	7.1	0.89 ± 0.13
CeTb1	5.3682	5.5 (6.9)	6.1	4.25 ± 0.75

[a] XRD results; fluorite-type cubic cell is considered. The Scherrer formula $x = 0.94\,\lambda/B\cos\theta$ is used to calculate particle sizes.[13] [b] Mean value of Feret diameter estimated from HREM images considering sets of 237, 192, and 182 particles for CeTb1, CeTb4, and CeO_2, respectively. Numbers in parentheses correspond to the volume weighted values. [c] XEDS average and error values estimated from measurements in five different zones of the particles.

g^{-1} at 77 K, followed by 30 min warming to RT, and 30 min outgassing at 77 K (residual pressure 1×10^{-4} mbar).

Isotopic exchange experiments were carried out with ca. 25 mg of sample held into a recirculating quartz reactor coupled to a grease-free standard vacuum system. The gas phase was analyzed with an on-line quadrupole spectrometer (Balzers QMG 421 C) connected to the reactor through a metering leak valve. Calcined samples (200 Torr of $^{16}O_2$ at 773 K for 1 h) were subjected to evacuation at reaction temperature (573 K, 10 min) and to a subsequent circulation of ca. 100 Torr of $C^{18}O_2$ at 573 K through the catalytic bed, with continuous analysis of gaseous products ($C^{18}O_2$, m/Z = 48; $C^{18}O^{16}O$, m/Z = 46; $C^{16}O_2$, m/Z = 44; and secondary masses).

III. Results and Discussion

Structural/Morphological Analysis. Transmission electron microscopy images at low magnification of the Ce−Tb mixed- oxide samples show for both samples the presence of polycrystalline aggregates of variable size in the range 0.1−1 μm. XEDS analysis of such aggregates show Ce/Tb atomic ratios close to 4 and 1 for CeTb4 and CeTb1, respectively (Table 1), in agreement with the chemical composition of the samples (see Experimental Section). A morphological and structural study of the mixed-oxide nanoparticles has been performed by analysis of several HREM micrographs of the samples. Figure 1 shows the nanocrystal particle size distributions obtained from an analysis employing Feret's diameters.[24] Average values obtained from this analysis are shown in Table 1. Characteristic HREM micrographs of the mixed-oxide samples are shown in Figure 2. Multi-faceted more or less rounded nanoparticles are apparently present for both samples. A Fourier analysis (using the SEMPER 6+ program for calculating fast Fourier transforms over selected regions of the digitized images) has been employed for characterization of lattice fringes in these images. Typical results obtained from this analysis are shown in the form of digital diffraction patterns (DDPs) in the insets of Figure 2. The spots observed in these DDPs correspond, in both cases, to spacing and angles characteristic of the fluorite structure typical for this type of oxides.[25] Most of the particles analyzed by this method appeared oriented along the [110] zone axis. Thus, *d* spacing values of 0.31 and 0.27 nm that correspond, respectively, to {111} and {002} type reflections of the ceria fluorite structure, are identified in the DDPs. It must be noted

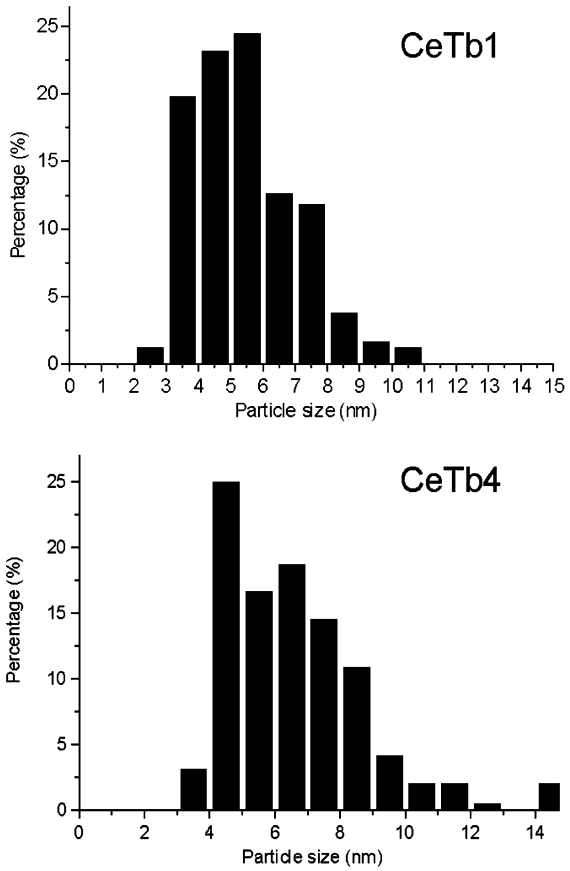

Figure 1. Histograms corresponding to the particle-size distributions obtained from HREM results for the Ce−Tb mixed-oxide samples.

that possible shifts in these values with respect to ceria, produced upon introduction of Tb cations into the fluorite structure of these nanostructured materials, are not discernible as they are within experimental error of this technique.

Powder X-ray diffraction patterns of the CeTb mixed-oxide samples, along with that obtained for the CeO_2 reference sample, are shown in Figure 3. Analysis of these results agrees with the existence of nanosize diffracting entities giving rise to fluorite-type patterns (indexed in the cubic $Fm3m$ space group) for the three samples (Table 1 and Figure 3). Although single-phase patterns are observed for the three samples, it must be noted that the relatively large width of the peaks obtained for these nanosize materials disallows extracting a definitive conclusion with respect to whether small amounts of segregated phases or concentration gradients within the mixed-oxide materials could be present at a more or less local level.

A negative shift of the lattice parameter (with respect to that of CeO_2), decreasing with the Tb content of the sample, is observed for the Ce−Tb mixed-oxide samples (Table 1). These shifts are relatively large in comparison with those (also negative) observed for other Ce−Tb mixed-oxide samples (up to ca. 30 atom. % Tb doping) prepared by co-decomposition of the nitrate precursors and sintered at 1473 K.[25] They are, however, fairly similar to the shifts observed for Ce−Tb mixed-oxide samples (up to 50 atom. % Tb doping) prepared by conventional coprecipitation and sintered at 1723 K.[26] The origin of these discrepancies must be due to

(24) Matyi, R. J.; Schwartz, L. H.; Butt, J. B. *Catal. Rev. Sci. Eng.* **1987**, *29*, 41.
(25) McBride, J. R.; Hass, K. C.; Poindexter, B. D.; Weber, W. H. *J. Appl. Phys.* **1994**, *76*, 2435.

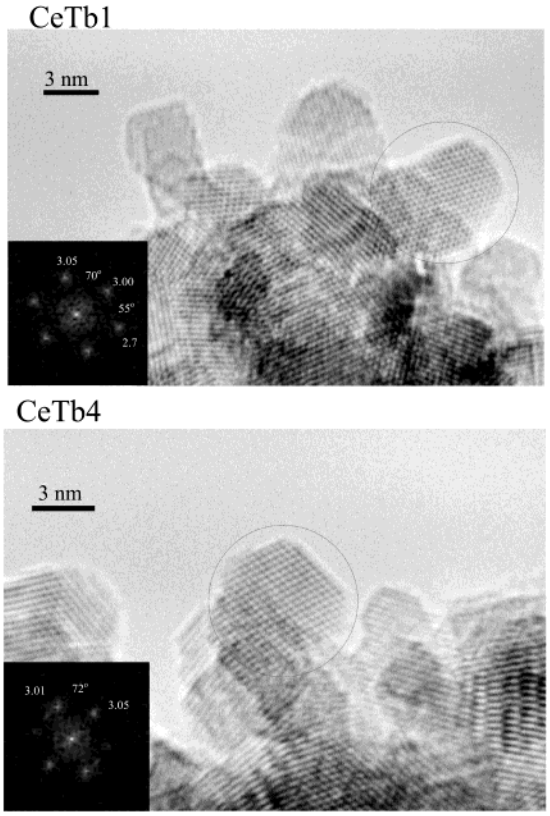

Figure 2. Representative HREM images of the Ce−Tb mixed-oxide samples. DDPs insets were obtained from the zones encircled in the images.

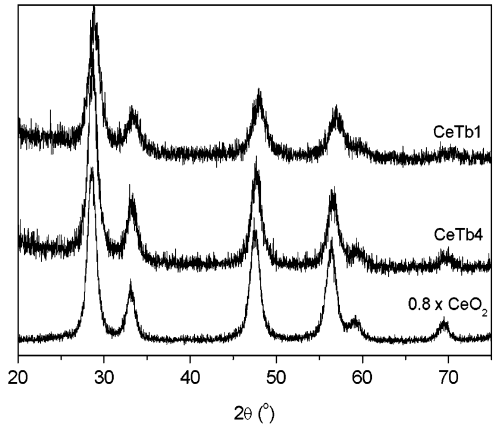

Figure 3. X-ray diffractograms of the Ce−Tb mixed-oxide samples and the CeO_2 reference.

differences in the relative amounts of M^{3+} cations (where M means either Ce^{3+} or Tb^{3+}), with the corresponding intrinsic oxygen vacancies associated with them, present in each case.[4,12,13,25] Thus, a correlation has been established between lattice parameter and ionic size of the cations present in the fluorite-type structure, which leads to lattice expansions upon substitution of M^{4+} cations (the corresponding ionic radii are 0.97 and 0.88 Å for Ce^{4+} and Tb^{4+}, respectively) by M^{3+} cations (1.14 and 1.04 Å are the ionic radii reported for Ce^{3+} and Tb^{3+}, respectively).[25] On this basis, the relatively large lattice contraction observed for the Ce−Tb mixed oxides prepared by microemulsion (Table 1), in comparison with the samples prepared by the other methods mentioned above, must be related to the relatively lower amount of M^{3+} cations (in our case, mainly related to Tb^{3+} cations, as suggested below by XPS data which show that cerium remains essentially as Ce^{4+}) present in the samples prepared by microemulsion. In this respect, considering the different sample preconditioning applied in each case, it must be considered that this may not be directly attributable to the specific preparation method employed but rather to the fact that that higher reduction levels appear to be favored upon increasing the sintering temperature of the materials.[26] It may be noted also that effects exclusively due to differences in particle size (i.e., without considering increases in the nonstoichiometry associated with formation of nanoparticles)[12] are not expected to lead to significant lattice contractions until very low sizes (below ca. 1 nm) are reached.[27] In any case, assuming that Vegard's rule is obeyed by the mixed oxides (i.e., that a linear change in the lattice parameter between those of pure CeO_2 and TbO_2 is achieved upon isomorphic Ce^{4+} substitution by Tb^{4+}),[3,4] the lattice parameters obtained for the CeTb mixed-oxide samples (Table 1) are larger than expected if the whole terbium appeared as Tb^{4+}, thus indicating that a part of the terbium is present as Tb^{3+} for both samples, and therefore that a proportional amount of intrinsic oxygen vacancies must be present in the samples for fulfilling electroneutrality requisites. A rough estimation of the amount of Tb^{3+} present in each sample can be done on the basis of the obtained lattice parameters and taking into account the corresponding cationic contents of each mixed-oxide sample (Table 1 and experimental). For this, it must be assumed that a linear correlation between the relative amount of Tb^{3+} and the lattice parameter for a determinate fixed atomic fraction of the dopant is fulfilled (Vegard's rule), and that a uniform distribution of the terbium cations has been achieved in the samples bulk. Then, considering[28] a lattice parameter of 5.213 Å for TbO_2 and that a lattice expansion of 0.0375 Å per atomic fraction of Tb^{3+} doping the CeO_2 lattice would be expected,[25] ca. 62 and 46% of the terbium would appear as Tb^{3+} for CeTb4 and CeTb1, respectively. This suggests a larger stabilization of the higher oxidation state of terbium as its bulk concentration is increased, in coincidence with results obtained for Ce−Tb mixed-oxide samples of significantly larger particle size.[11]

The presence of oxygen vacancies in the Ce−Tb mixed-oxide samples is also inferred from analysis of the Raman spectra (Figure 4). The spectrum of CeO_2 is mainly constituted by a narrow and slightly asymmetric band at 462 cm^{-1} with faint bands or shoulders being appreciated at ca. 270 cm^{-1} and in the 530−700 cm^{-1} range. A slight blue shift of the main band (to 463 cm^{-1}) is observed for sample CeTb4, which in turn shows a weak band at 258 cm^{-1} and a broad one in the 530−700 cm^{-1} range displaying a maximum at ca. 560 cm^{-1}. A higher blue shift of the main band (to 468 cm^{-1}) is observed for CeTb1 and a broad band is also detected in the 530−700 cm^{-1} range, while weak and poorly defined bands appear to be present at ca. 255 and 295

(26) de Vries, K. J.; Meng, G.-Y. *Mater. Res. Bull.* **1998**, *33*, 357.

(27) Cordatos, H.; Ford, D.; Gorte, R. J. *J. Phys. Chem.* **1996**, *100*, 18128.

(28) Gruen, D. M.; Koehler, W. C.; Katz, J. J. *J. Am. Chem. Soc.* **1951**, *73*, 1475.

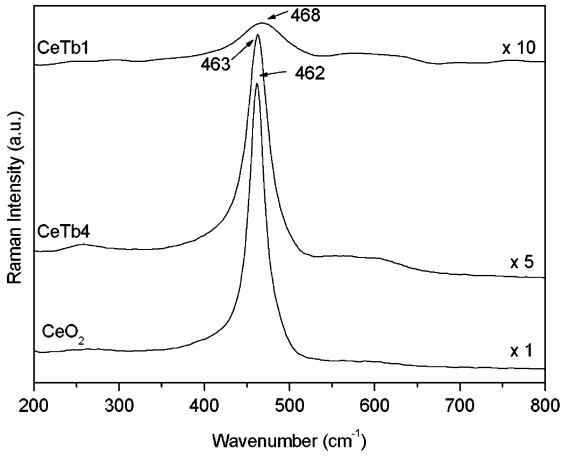

Figure 4. Raman spectra of the indicated samples.

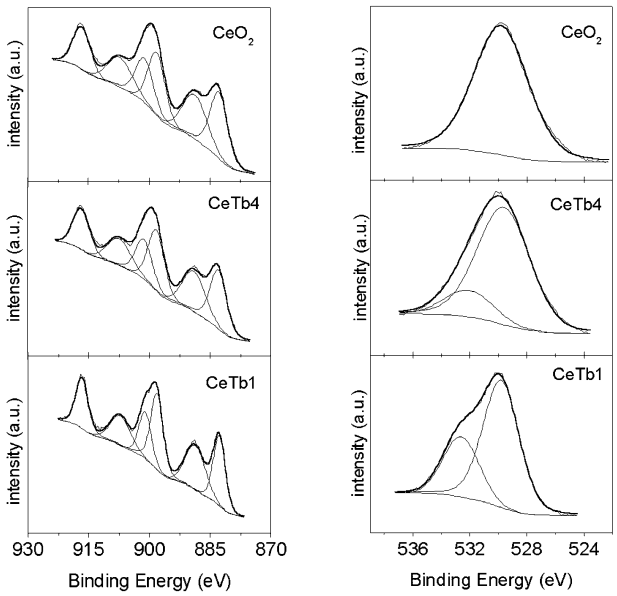

Figure 5. Ce(3d) (left) and O(1s) (right) XPS spectra and fittings of the indicated samples.

cm^{-1}. It may be noted that the overall intensity of the spectrum decreases with increasing the Tb content. This is presumably related to the corresponding decrease in the sampling depth due to increasing absorption at or near the frequency of the exciting laser as the terbium content, and consequently the nonstoichiometry, is increased;[25,29] this can also result as a consequence of sample heating on exposure to the exciting laser but this is less likely to be relevant on the basis of the absence of shifts in the frequency of the main band when collecting spectra at different exciting power in the 10−100 mW range for CeTb4 and CeO_2, the best band resolution being achieved at the highest power. It is also possible to appreciate an increase, with respect to CeO_2, in the ratio of intensities between the band in the 530−700 cm^{-1} range and the main band for both CeTb samples. This apparently occurs to a higher extent for CeTb1. This has been shown to be related to the presence of oxygen vacancy defects[13,25] in qualitative agreement with the discussion in the former paragraph. This can also explain the increasing line width of the main band observed with increasing the Tb content,[25] although effects of phonon confinement and inhomogeneous strain (that can be associated to compositional or redox heterogeneities as a function of the particle size) can also contribute to a small extent to this observation.[13] The main band at 462−468 cm^{-1} is related to the first-order peak of F_{2g} symmetry which is, to a first approximation, the only allowed Raman mode for fluorite structured oxides;[13,25,30] as it occurs in the spectra shown in Figure 4, other second-order peaks can appear in the ca. 250−350 cm^{-1} range of these materials,[13] although these can be also related to surface phonons.[31] According to previous detailed analysis of Raman spectra of ceria and doped-ceria samples,[13,25] the main factors that affect the frequency of the F_{2g} mode are the lattice strain and the presence of vacancies while phonon confinement plays a more limited role. Taking these factors into account, the shift observed for the main band in the Ce−Tb mixed oxides (Figure 4) must be related to a balance of opposite factors. Thus, a larger blue shift would be expected for both mixed oxides (to a larger extent for CeTb1) upon application of the Grüneisen parameter (employed for estimating the shift as a function of lattice strain, using a similar approach as done elsewhere)[13,25] to the lattice contractions observed by XRD (Table 1). This must be compensated by the presence of oxygen vacancies, which, as a particularity of those associated with the terbium dopant, appear to produce red shifts on the main band.[25] On the other hand, the presence of vacancies can have also a role in the asymmetric shape observed for the main band,[25] although the inhomogeneous strain can have a major contribution on this.[13]

XPS spectra were obtained at the Ce(3d), O(1s), C(1s), and Tb($3d_{3/2}$) zones of the oxidized samples; the first two ranges are shown in Figure 5. Compositional analysis of the mixed oxides yields atomic ratio values of Tb/Ce = 0.358 and 1.275 for CeTb4 and CeTb1, respectively, which are somewhat higher than chemical analysis or XEDS values (Experimental Section and Table 1); this suggests that a certain Tb enrichment may be produced at the surface of the mixed oxides, although it must be noted that the important uncertainty in the atomic sensitivities reported in the literature for Tb may affect these values.[21] Similar Ce(3d) XPS spectra have been obtained for the two Ce−Tb mixed oxides and the CeO_2 reference (Figure 5). Peaks' fitting is consistent with the almost exclusive presence of Ce^{4+} species in them, in agreement with the 12.49, 13.43, and 14.68% values of the integrated area contribution of the u‴ peak (appearing at 916.7 eV) to the whole Ce(3d) spectrum observed for CeO_2, CeTb4, and CeTb1, respectively.[4] It can be noted that the spectra of the CeO_2 and CeTb4 samples display significantly larger line widths than those of CeTb1. This is probably due to a more important charging effect in the two former samples (indeed, the charging correction needed in the binding energy values was significantly larger for them), which in turn indicates a higher electronic conductivity in CeTb1, consistent with values reported in the literature for Ce−Tb mixed-oxide samples of larger particle size.[11] Analysis of the O(1s) zone shows a main peak at ca. 529.8 eV for the three samples, attributable to bulk oxide ions.[4,23,32] Noteworthy, a shoulder at ca. 2.8 eV higher binding

(29) Xie, S.; Iglesia, E.; Bell, A. T. *J. Phys. Chem. B* **2001**, *105*, 5144.
(30) Keramidas, V. G.; White, W. B. *J. Chem. Phys.* **1973**, *59*, 1561.
(31) Wang, S.; Wang, W.; Zuo, J.; Qian, Y. *Mater. Chem. Phys.* **2001**, *68*, 246.

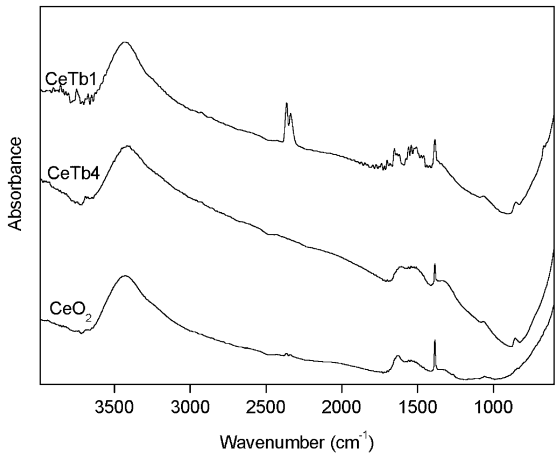

Figure 6. Infrared spectra of the samples diluted in KBr.

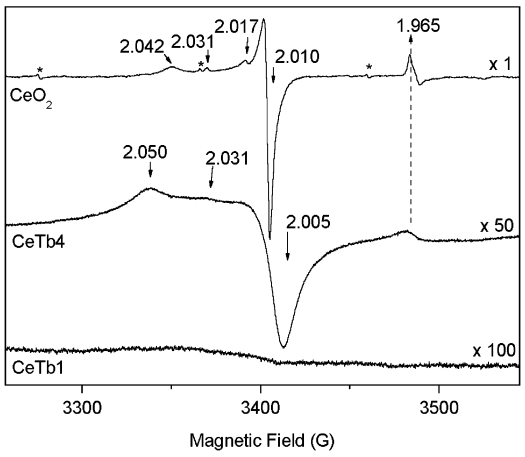

Figure 7. O_2-probe EPR spectra of the indicated samples. Signals marked with an asterisk correspond to residual Mn^{2+} impurities.

energy appears when Tb is present, growing with its concentration. One possible cause of such feature is the presence of carbonate species (whose existence has been detected in infrared spectra, in which these species appear in the 1700−800 cm^{-1} range, Figure 6). Verification of this by examining the C(1s) region (not shown) is difficult, as the Tb($4p_{3/2}$) (multipeaked)[33] and Ce(4s) lines severely overlap it; still, the intensity increase in the region around 289 eV is lower than what would be expected, considering the relative atomic sensitivities, if the O(1s) shoulder corresponded to carbonates, so this latter hypothesis seems unlikely as sole explanation of the presence of this shoulder. Other alternatives are the attribution to oxide ions in the close environment of clustered vacancies and/or to oxygen species belonging to hydroxyl groups present in the sample (according to the presence of relatively intense bands in the 4000−3000 cm^{-1} range of the infrared spectra of the samples, Figure 6).[23,32] An independent experiment showing a decrease of ca. 40% in the shoulder component at 532.6 eV upon outgassing CeTb1 at 773 K (data not shown) along with experiments of H_2O adsorption on TbO_x suggest that such a line can mainly be related to a specific type of hydroxyl groups coordinated to Tb cations.[34] Unfortunately, the large width of the hydroxyls band detected in the IR spectra of the three samples (related to the major presence of hydroxyls affected by H-bonds and/or corresponding to a hydration layer) does not allow discernment of differences in this respect. On the other hand, the main Tb($3d_{3/2}$) feature in the XPS spectra of the mixed oxides (showing a somewhat asymmetric band centered at 1276.4 eV; data not shown) is similar in both Ce−Tb samples, and no definitive conclusion can be extracted from it with respect to the redox state of terbium.

Surface and Oxygen Handling Properties. O_2-probe EPR spectra of the CeTb mixed oxides and of the CeO_2 reference are shown in Figure 7. Two superoxide signals (formally O_2^-−Ce^{4+} species) are observed in the spectrum of CeO_2:[35,36] a major one at $g_{||} = 2.042$ and $g_\perp = 2.010$ (signal OC1), and a minor one at $g_z = 2.031$, $g_x = 2.017$, and $g_y = 2.011$ (signal OC2). Other minor signals due to residual Mn^{2+} impurities and to trapped electron defects or residual Cr^{3+} impurities (feature at $g = 1.965$),[37] typically present in ceria samples at the ppm or sub-ppm level,[4] are also observed in the spectrum and were already present prior to oxygen adsorption. Important changes are observed in the spectra upon Tb doping. Thus, a significant intensity decrease of oxygen-derived signals is observed for both samples and most specially for CeTb1, which shows only a very broadened and flattened absorption in the zone corresponding to this kind of species, making it impossible to resolve any feature of the signals eventually present. The spectrum of CeTb4 shows mainly the presence of a signal OC1′ at $g_{||} = 2.050$ and $g_\perp = 2.005$ (attributed to O_2^-−Ce^{4+} species)[35,36] and a minor signal OC2. The presence of a small broadened feature at $g = 1.965$ is also detected for this sample. Concerning detection of either Tb^{4+} or Tb^{3+} in the mixed oxides, only a broad and weak feature at $g \approx 5.0$ (that may be attributed to Tb^{4+} species)[38] is present for CeTb4, indicating that the majority of these cations are subjected to strong magnetic relaxation phenomena and escape detection at 77 K. The significant broadening of signal OC1′ and of the feature at $g = 1.965$ in CeTb4 indicate the presence of strong magnetic interactions with Tb^{3+} or Tb^{4+} cations (both showing a paramagnetic character in doped ceria).[39] Such interaction is most likely very strong in CeTb1, hindering detection of paramagnetic species under the employed conditions. In any case, the evolution of O_2^-−Ce^{4+} species (in particular, the shift of g_z to 2.050) suggests that the presence of Tb cations at the sample surface can induce a higher degree of coordinative unsaturation around the surface Ce cations,[35,36] which may be of relevance for reactions such as those involving coupling of NO molecules.[40]

To get more hints on the surface structure of these samples, infrared experiments have been performed

(32) Holgado, J. P.; Munuera, G.; Espinós, J. P.; González-Elipe, A. R. *Appl. Surf. Sci.* **2000**, *158*, 164.
(33) Paladia B. D.; Lang, W. C.; Norris, P. R.; Watson, L. M.; Fabian, D. J.; *Proc. R. Soc. London A* **1977**, *354*, 269.
(34) Munuera, G. Personal communication.
(35) Soria, J.; Martínez-Arias, A.; Conesa, J. C. *J. Chem. Soc., Faraday Trans.* **1995**, *91*, 1669.
(36) Martínez-Arias, A.; Fernández-García, M.; Belver, C.; Conesa, J. C.; Soria, J. *Catal. Lett.* **2000**, *65*, 197.
(37) Figaj, M.; Becker, K. D. *Solid State Ionics* **2001**, *141*−*142*, 507.
(38) Ebendorff-Heidepriem, H.; Ehrt, D. *J. Phys.: Condens. Matter* **1999**, *11*, 7627.
(39) Greznev, Y. S.; Zaripov, M. M.; Stepanov, V. G. *Sov. Phys.-Sol. St.* **1965**, *7*, 2937.
(40) Martínez-Arias, A.; Soria, J.; Conesa, J. C.; Seoane, X. L.; Arcoya, A.; Cataluña, R. *J. Chem. Soc., Faraday Trans.* **1995**, *91*, 1679.

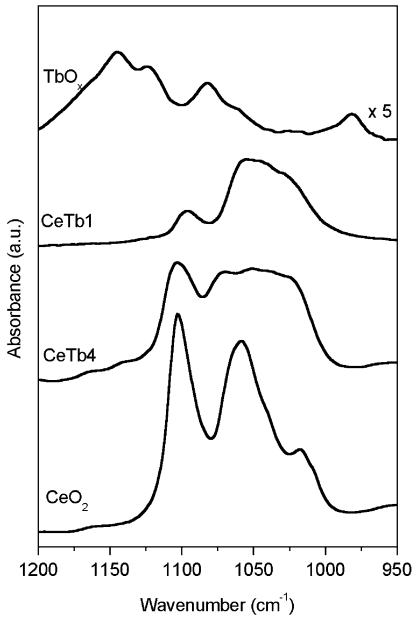

Figure 8. Infrared spectra at the ν_{O-C} region of methoxy species chemisorbed on the indicated samples.

employing methanol as probe molecule, according to a methodology described elsewhere.[41−43] Spectra in the ν(O−C) stretching zone of the species formed upon methanol adsorption on the two mixed-oxide samples, as well as on the two reference samples, are shown in Figure 8. The spectrum of CeO_2 is similar to that observed for other ceria samples in the oxidized state[41−43] and exhibits a set of bands at 1102 cm^{-1} (type I band), 1059 cm^{-1} (with a red shoulder at ca. 1042 cm^{-1}; type II bands) and 1018 cm^{-1} (with a red shoulder at ca. 1008 cm^{-1}; type III bands). These bands can be attributed to the ν(O−C) stretching vibration of chemisorbed methoxy species formed upon methanol dissociation on the sample surface.[41−43] Type I, II, and III bands can be assigned to, respectively, on-top, doubly bridging, and triply bridging methoxy species adsorbed on the sample surface.[42] Significant changes are produced in the spectra upon doping with terbium. First, a new type I band appears and apparently shifts to lower frequency with increasing terbium content. Thus, in this spectral zone, the spectrum of CeTb4 shows the overlapping of the band at 1102 cm^{-1} with another one (appearing as a shoulder) at ca. 1098 cm^{-1}, while CeTb1 shows only a band at 1096 cm^{-1}. Second, in a similar way, bands due to type III methoxy species apparently shift to higher frequency with increasing terbium content, appearing at ca. 1025 cm^{-1} for CeTb4 and at 1029 cm^{-1} (with a red shoulder at ca. 1025 cm^{-1}) for CeTb1. The situation appears more complex in the zone corresponding to type II methoxy species in which the spectra of both CeTb4 and CeTb1 show the overlapping of different (not fully resolved) bands. Noteworthy, the intensity ratio between type II−III bands and type I bands increases with increasing the terbium content of the sample. On the other hand, no correlation is observed between bands observed for any of the Tb-doped samples and those of the terbia reference.

These results suggest a modification of the close environment of cationic cerium adsorption sites as a consequence of the presence of terbium cations, suggesting, in turn, that mixed-oxide surface structures are present in which at least cerium cations appear exposed at the surface of the two mixed-oxide samples. Thus, the shifts observed for type I and III methoxy bands upon Tb doping are fairly similar to those observed upon doping of ceria samples with zirconium and which were attributed to formation of Ce−Zr mixed-oxide surface structures.[42] In the same sense, observation of different bands in the zone corresponding to type II methoxy species for the Tb-doped samples suggests the presence of new bridging adsorption sites in which both cerium and terbium cations are involved. A further complication with respect to the new spectral features appearing in this case lies in the possibility that two different oxidation states of terbium are present at the sample surface. Unfortunately, analysis of the C−H stretching zone of the adsorbed methoxy species does not provide further information with respect to the nature of the adsorption sites in these samples because multiband spectra displaying overlapping bands difficult to fully resolve, and whose analysis is beyond the scope of this work, are observed for both samples. On the other hand, the increasing intensity ratio between bands of types II−III and type I observed with increasing Tb content suggests, on the basis of the similar trend observed upon reduction of ceria samples,[43] that a significant degree of coordinative unsaturation is achieved (upon outgassing at 773 K) in the environment of cationic cerium centers upon Tb doping, in agreement with the results observed by O_2-probe EPR experiments (Figure 7).

Oxygen isotopic exchange experiments using labeled $C^{18}O_2$ were carried out to study the characteristics of oxygen diffusion in the bulk of these samples; after the work by Kakioka et al. and Martin and Duprez, these data can be conveniently used to obtain a measure of the bulk diffusion coefficient.[44,45] Bulk oxygen coefficient (D_b) is calculated according to the model by Kakioka et al.[44]

$$\mathrm{Ln}(F^{18}O_g - F^{18}O_s) = -C_1 D_b^{1/2} t^{1/2} + C_2 \qquad (1)$$

where $F^{18}O$ corresponds to ^{18}O fractional percentage in the gas phase (g) and initial in the solid (s), t is time, and the C_x are constants; for the estimation of D_b in experiments comparing different samples, it must be taken into account the dependence of C_1 on the specific surface area and the bulk oxygen density (taken from the experimental part and XRD results).[44] When $C^{18}O_2$ is contacted with the solid, surface exchange via adsorption−desorption of carbonate species must occur initially; this corresponds to the first part of the curves displayed in Figure 9. Further exchange of oxygen (after surface equilibration) can only proceed at the bulk of the specimen and, according to eq 1, would obey a linear relationship between its logarithmic form and the

(41) Binet, C.; Daturi, M.; Lavalley, J.-C. *Catal. Today* **1999**, *50*, 207.
(42) Daturi, M.; Binet, C.; Lavalley, J.-C.; Galtayries, A.; Sporken, R. *Phys. Chem. Chem. Phys.* **1999**, *1*, 5717.
(43) Daturi, M.; Finocchio, E.; Binet, C.; Lavalley, J.-C.; Fally, F.; Perrichon, V.; Vidal, H.; Hickey, N.; Kašpar, J. *J. Phys. Chem. B* **2000**, *104*, 9186.
(44) Kakioka, H.; Ducarme, V.; Teichner, S. J. *J. Chim. Phys.* **1971**, *68*, 1715.
(45) Martin, D.; Duprez, D. *J. Phys. Chem. B* **1996**, *100*, 9429.

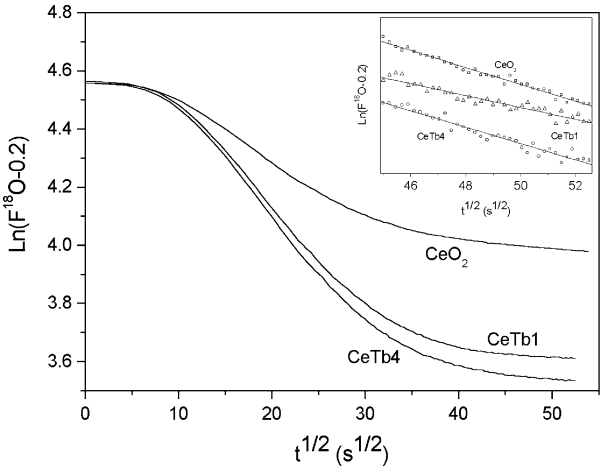

Figure 9. Logarithm of ^{18}O fractional percentage at the gas phase vs square root of time obtained during isotopically labeled carbon dioxide exchange at 573 K over the indicated samples. A value $F^{18}O(s) = 0.2\%$ (natural abundance) has been taken for the initial value of $F^{18}O$ in the solid. The inset shows a detail of the linear zone employed for estimation of bulk diffusion coefficients (see text for details).

Table 2. Coefficients for Oxygen Bulk Diffusion at 573 K (See Text for Details)

sample	D_b (10^{-21} cm^2 s^{-1})
CeO_2	44
CeTb4	34
CeTb1	21

square root of time. It must be noted that although the accuracy of the bulk oxygen diffusion values obtained by this method may be subject to discussion, the trends detected have been shown to correlate well with the ease in the management of oxygen by the bulk of the material.[18,44−47]

Results using this analysis are shown in Table 2. They suggest that Tb doping of ceria in the amounts employed for the two examined samples produces a slight decrease of the oxygen bulk mobility in these nanosized particles. In ceria-related systems, oxygen-ion mobility depends on the concentration, charge, and mobility of the carriers, e.g., electrons or Ce^{3+}, holes, and anion vacancies.[48] The above inferred presence of Tb^{3+} in fully oxidized samples induces the existence of anion vacancies to achieve charge neutrality (in accordance with Raman results) and would thus be expected to enhance oxygen exchange and mobility.[11] However, as shown in many of the Ce-containing systems,[48] a maximum is observed in anionic conductivity as a function of the dopant concentration. This is frequently explained on the basis of a hypothetical interaction between defects, probably originating from the presence of ordering at a local level (i.e., dopant cation-vacancy associations).[48] Indeed, for Ce−Tb mixed-oxide samples of large particle size a maximum ionic conductivity has been observed at 0.25 atomic fraction of the Tb dopant.[11] Therefore, for the nanosized mixed-oxide particles it would appear that such maximum may occur at lower Tb atomic fraction and/or that a gradual decrease of oxygen mobility is produced with Tb doping (at least up to 0.5 Tb atomic fraction).

Conclusions

Two Ce−Tb mixed-oxide samples (with ca. 4 and 1 Ce/Tb atomic ratios) have been prepared by a microemulsion method, characterized, and examined with respect to their oxygen handling properties (oxygen interaction with the surface of outgassed samples, studied with EPR, and oxygen bulk diffusion examined by an isotopic exchange method). High-surface-area materials constituted by agglomerates of nanoparticles (average size in the 5−7 nm range) with fluorite structure are formed. Both samples show the presence of oxygen vacancies attributed to the presence of Tb^{3+} in a relative amount that decreases with increasing the Tb content of the mixed oxide. Oxygen adsorption at room temperature on the samples outgassed at 773 K generate superoxide species whose analysis (by EPR) reveals a Tb-induced trend of the nanoparticles toward formation of clustered vacancies defects at their surface, also in agreement with adsorbed methoxy IR experiments. This may have interesting catalytic implications because, for instance, those defects are proposed to be most active in NO reduction processes.[40] On the other hand, the oxygen bulk diffusion coefficient is shown to decrease gradually with increasing the Tb content of the mixed-oxide nanoparticles.

Acknowledgment. Thanks to Prof. G. Munuera for helpful comments and discussions on the XPS results. Dr. M. Faraldos, Mr. F. Sánchez, and Mr. E. Pardo are acknowledged for performing ICP-AES analysis, EPR, and XPS experiments, respectively. The HREM images were obtained at the E.M. facilities at the Universidad de Cádiz; A.B.H. wishes to thank Drs. J. J. Calvino, C. López-Cartes, and J. A. Pérez-Omil for their kind and patient help during performance of the HREM studies. Support from CICYT (Project MAT 2000-1467) is fully appreciated.

CM031028N

(46) Guerrero-Ruiz, A.; Rodríguez-Ramos, I.; Ferreira-Aparicio, P.; Volta, J. C. *Catal. Lett.* **1997**, *45*, 113.
(47) Fernández-García, M.; Martínez-Arias, A.; Guerrero Ruiz, A.; Conesa, J. C.; Soria, J. *J. Catal.* **2002**, *211*, 326.
(48) Trovarelli, A., Ed. *Catalysis by Ceria and Related Materials*; Imperial College Press: London, 2002; Ch. 2.